Polarization-independent efficiency enhancement of organic solar cells by using 3-dimensional plasmonic electrode

Xuanhua Li,[1] Wallace C. H. Choy,[1,a)] Xingang Ren,[1] Jianzhuo Xin,[2] Peng Lin,[1] and Dennis C. W. Leung[2]

[1]*Department of Electrical and Electronic Engineering, The University of Hong Kong, Pokfulam Road, Hong Kong*

[2]*Department of Applied Physics, The Hong Kong Polytechnic University, Hung Hom, Kowloon, Hong Kong*

(Received 18 February 2013; accepted 5 April 2013; published online 17 April 2013)

Plasmonic back reflectors have recently become a promising strategy for realizing efficient organic solar cell (OSCs). Since plasmonic effects are strongly sensitive to light polarization, it is highly desirable to simultaneously achieve polarization-independent response and enhanced power conversion efficiency (PCE) by designing the nanostructured geometry of plasmonic reflector electrode. Here, through a strategic analysis of 2-dimensional grating (2D) and 3-dimensional patterns (3D), with similar periodicity as a plasmonic back reflector, we find that the OSCs with 3D pattern achieve the best PCE enhancement by 24.6%, while the OSCs with 2D pattern can offer 17.5% PCE enhancement compared to the optimized control OSCs. Importantly, compared with the 2D pattern, the 3D pattern shows a polarization independent plasmonic response, which will greatly extend its uses in photovoltaic applications. This work shows the significances of carefully selecting and designing geometry of plasmonic nanostructures in achieving high-efficient, polarization-independent plasmonic OSCs. © *2013 AIP Publishing LLC* [http://dx.doi.org/10.1063/1.4802261]

Light trapping is an important topic for thin film organic solar cells (OSCs) to improve the light absorption and thus performances of OSCs.[1–5] Recently, light-trapping schemes based on patterned electrodes have been reported by using nanopatterned front substrate or buried metallic back reflector to couple incident light into guided modes, propagating along the plane of absorbing layer.[6–14] The integration of patterned front electrode (i.e., ITO) is realized in OSCs, and efficient light harvesting has been achieved.[6,7] However, the formation of organic layer and thus the performance is very sensitive to the roughness and geometries of substrate.[7] As an alternative, highly promising light trapping strategy is to utilize periodic nanostructured back reflectors in OSCs.[4] By carefully selecting the geometry, this approach is capable of providing significant enhancement of the optical path length within the thin absorber layer.[15–17] Very recently, our group also demonstrated efficient improvement in optical absorption by using 2D Ag grating electrode as a back reflector in inverted OSCs.[4] According to theoretical and experimental results, the excited surface plasmon resonances (SPRs) and the couplings between SPRs with other optical modes of the device structures significantly contribute to near-field enhancement and thus absorption improvement of OSCs.[4]

SPRs are strongly correlated with light polarization.[9,10,15,18–22] For practical applications, it is highly desirable for plasmonic OSCs to have a polarization-independent response, which will significantly improve their performance and greatly extend their use in solar applications.[10,19,22] Unfortunately, the previously 2D plasmonic grating solar cell strongly depends on the polarization due to the asymmetry of the structures.[9,18,21,23] Thus, carefully selecting and designing geometry of plasmonic nanostructures in simultaneously achieving both enhanced power conversion efficiency (PCE) and polarization-insensitivity OSCs are still challenging.

In this work, we will investigate a periodic structure which will simultaneously offer both the polarization-independent plasmonic properties and enhancement of PCE. Through a strategic comparison of 2D and 3D patterns (see the schematics in Figs. 1(a) and 1(c)) with similar periodicity as a plasmonic back reflector in inverted OSCs, we demonstrate that the proposed OSCs with 3D patterned anode can show a larger light-trapping effect and a more efficient PCE enhancement by 24.6%. Moreover, compared with the 2D grating design, the 3D patterned design shows a polarization-independent response due to the symmetric arrangement of 3D patterned geometry utilized as the back reflector.

The planar and patterned inverted OSCs with a structure of ITO/TiO_2 (20 nm)/active layer (120 nm)/MoO_3 (10 nm)/Ag (with or without pattern) (100 nm) have been investigated (Figs. 1(a) and 1(c)). For device fabrication, polymer blends of P3HT: $PC_{60}BM$ (1:0.8, wt. %/wt. %, 15 mg/ml) in chlorobenzene was spin-coated at 670 rpm for 50 s on top of the TiO_2 layer. The active layer thickness is about 120 nm. To obtain the 2D and 3D pattern on the active layer, the polydimethylsiloxane (PDMS) nanoimprinted method was applied onto the surface of the active layer.[4,13] By the removal of the PDMS mold, MoO_3 (10 nm) and silver (100 nm) layers were thermally evaporated onto the active layer pattern at a pressure of 10^{-6} Torr. Similarly, for the planar control device, the flat PDMS mold was also applied on the active layer.

The atomic force microscope (AFM) images of P3HT:PCBM film with 2D and 3D patterns are measured using Asylum Research MFP-3D in tapping mode as shown in Figs. 1(b) and 1(d). As shown in the AFM images, two

a)Author to whom correspondence should be addressed. Electronic mail: chchoy@eee.hku.hk

 © 2013 AIP Publishing LLC

Downloaded 17 Apr 2013 to 147.8.236.116. This article is copyrighted as indicated in the abstract. Reuse of AIP content is subject to the terms at: http://apl.aip.org/about/rights_and_permissions

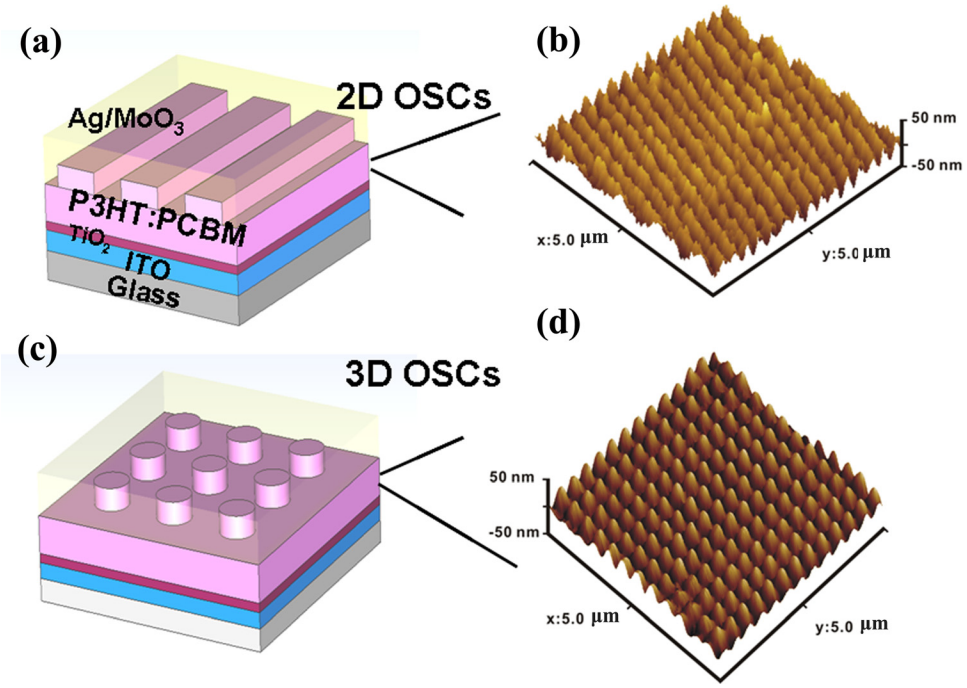

FIG. 1. The schematics of (a) 2D OSCs and (c) 3D OSCs, the AFM images of active layer with (b) 2D nanograting and (c) 3D nanopattern.

types of nanostructures both have the similar periodicity and depth with ~350 nm and 55 nm, respectively. The big difference is from geometry. As observed, the 2D grating have obvious linear direction, but the 3D array of nanopillar shows square-symmetrically distributed nanostructures arrangement (with x- and y-axis symmetry). When the Ag anode is subsequently evaporated on the three different nanostructured active layer surfaces, including planar active layer, 2D active layer, and 3D active layer, the anode/active layer interface closely follows the surface profile of the active layer. Hence the planar and nanopatterned features are preserved on the Ag anode, which indicate OSCs with three types of metallic back reflectors could be obtained. Through a comparison of 2D and 3D patterns with similar periodicity as a plasmonic back reflector in inverted OSCs, we will show the significances of carefully selecting and designing geometry of plasmonic nanostructures for achieving high-efficient, polarization-independent plasmonic OSCs.

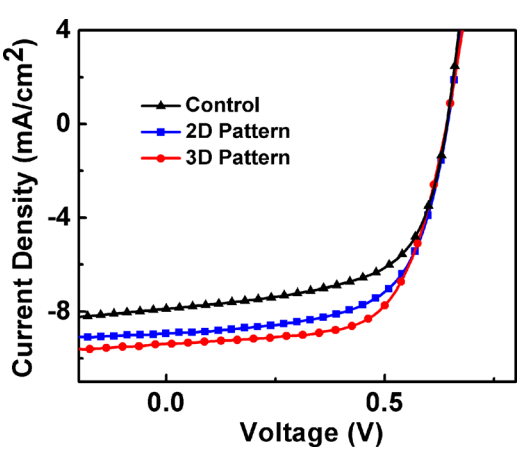

FIG. 2. Current density-voltage (J-V) characteristics of devices with or without nanopatterned back reflector measured under AM 1.5 illumination at 100 mW/cm^2.

Fig. 2 presents current density-voltage (J-V) characteristics of the cells with and without nanostructured back reflector, with their performance summarized in Table I. First, the optimized reference device shows PCE of 3.09%, and PCE improves to 3.62% by applying a 2D nanograting in OSCs. Interestingly, the PCE reaches 3.85% when a 3D nanopatterned back reflector is adopted in OSCs. As a result, compared to the control OSCs, the proposed OSCs with 3D array anode enhance PCE by 24.6%, while the OSCs with 2D grating device improve PCE by 17.5%, which means the geometry of back reflector in OSCs will strongly affect the device performances.

For the 2D and 3D pattern devices, PCE improvements are attributed to J_{sc} and fill factor (FF) increments, while V_{oc} keeps similar to that of the control device. The J_{sc} values of OSCs with 2D and 3D pattern are 8.93 and 9.31 mA cm^{-2} with 14.72% and 18.15% enhancement, respectively, compared to the control OSC ($J_{sc} = 7.88$ mA cm^{-2}). The higher FF can be explained by the increased interfacial area between active layer and electrode as well as the decreased R_s.[4,8,24] The interfacial area at the OSCs with 2D and 3D patterns increase by a factor of 1.25 and 1.41, respectively (ratio: increased area related to initial area with a planar surface).

To understand the origin of the J_{sc} increment, we extract the absorption from the diffuse reflection (R) and transmission (T), using 1-R-T. As shown in Fig. 3(a), we find that there is a clear increment of absorption when the 2D and 3D

TABLE I. Photovoltaic parameters of the OSCs with or without nanopatterned back reflector under AM 1.5G illumination at 100 mW/cm^2. R_S is derived from the slope of the current–voltage (J-V) curves under dark at 1 V.

Device	V_{OC} (V)	J_{SC} (mA/cm^2)	FF (%)	PCE (%)	R_S (Ω cm^2)
Flat (control)	0.64	7.88	0.608	3.09 ± 0.15	3.5
2D pattern	0.64	8.93	0.635	3.63 ± 0.25	1.8
3D pattern	0.64	9.31	0.647	3.85 ± 0.25	1.2

Downloaded 17 Apr 2013 to 147.8.236.116. This article is copyrighted as indicated in the abstract. Reuse of AIP content is subject to the terms at: http://apl.aip.org/about/rights_and_permissions

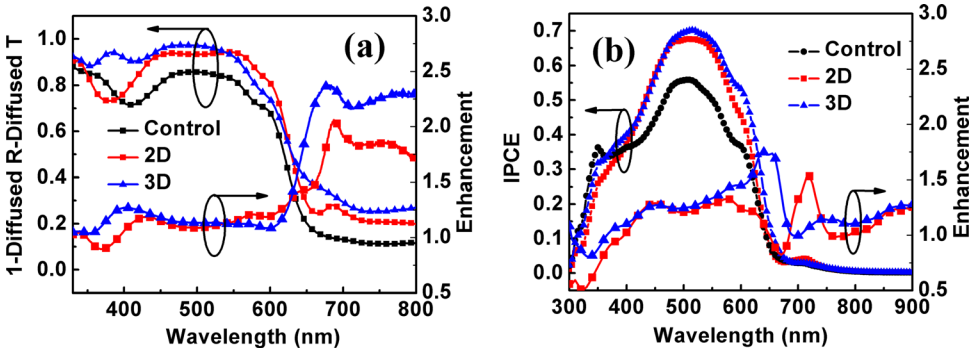

FIG. 3. (a) The extracted absorption of OSCs (1-diffused reflection (R)-diffused transmission (T)) with and without nanopatterned back reflector and the absorption enhancement, i.e., (1-R-T of 2D and 3D OSCs)/(1-R-T of control flat OSC). (b) IPCE of the three OSCs and the enhancement, i.e., (IPCE of patterned OSC)/(IPCE of control flat OSC).

Ag patterned reflectors are introduced to the OSCs. To further clarify our results, we calculate the absorption enhancement by dividing the absorption of the nanopatterned devices by that of the control planar device. For 2D Ag grating device, relative absorption enhancement >1 are observed over a broad spectral range from 430 to 800 nm, with peaks of ~2 (i.e., double the absorption) at 700 nm. For the 3D Ag nanopatterned device, we find an obvious absorption enhancement peak at 650 nm along with a broad absorption enhancement region. Regarding the absorption enhancement peaks of 2D (at ~700 nm) and 3D (at ~650 nm) devices, we could attribute them to the excited SPR mode induced by the metallic back reflector from our theoretical studies as shown in Fig. 4. For 2D grating OSCs, the strong absorption peak at about 700 nm can be explained by the SPR excited by TM polarized light (Fig. 4(a)). For 3D nanopatterned OSCs, the strong SPR mode can be excited by both the TE and TM polarized light with wavelength of 650 nm (Figs. 4(c) and 4(d)). Furthermore, compared with 2D grating OSC, 3D patterned one can trap more light into the active layer as shown in Figs. 3(a) and 4, which indicates the 3D patterned structure is the better plasmonic back reflector. As a result, the J_{sc} and PCE enhancement for the 3D device become more observable compared to those of 2D device.

To further demonstrate the effects of plasmonic nanopatterned back reflector on the performances of OSCs, the

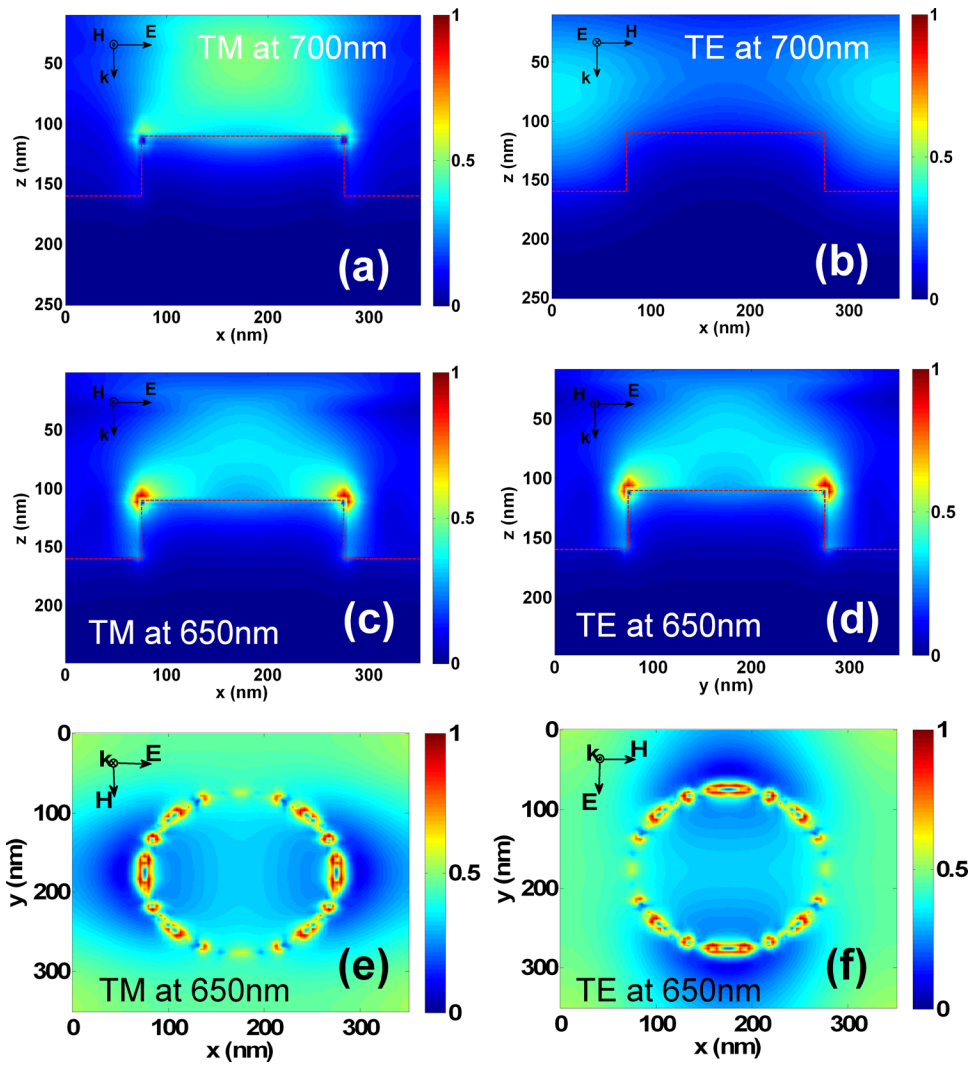

FIG. 4. The normalized near field (|E|) profiles of OSCs with metal patterns with respect to the maximum value of that of the 3D OSCs. Cross-section near-field profile of (a) TM polarized light and (b) TE polarized light at 700 nm for 2D grating OSC, cross-section near-field profile of (c) TM polarized light and (d) TE polarized light at 650 nm for 3D patterned OSC, and top view near-field profile of (e) TM polarized light and (f) TE polarized light at 650 nm for 3D patterned OSC.

Downloaded 17 Apr 2013 to 147.8.236.116. This article is copyrighted as indicated in the abstract. Reuse of AIP content is subject to the terms at: http://apl.aip.org/about/rights_and_permissions

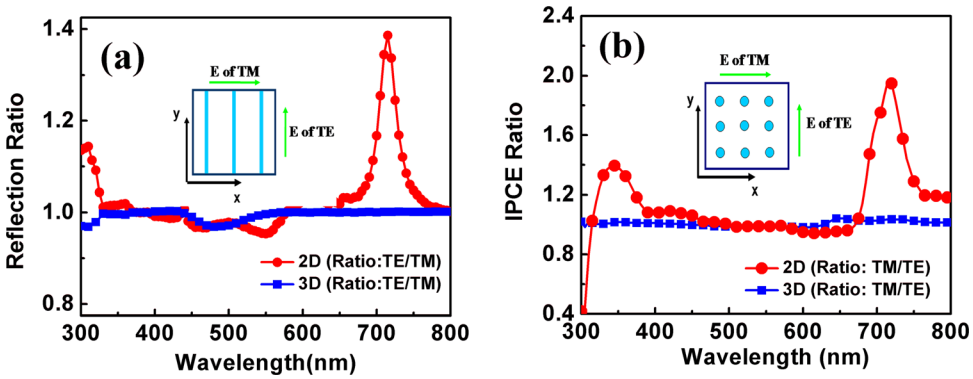

FIG. 5. (a) The reflection ratio of OSCs for TE and TM polarized incident light, and (b) IPCE ratio of OSCs for TE and TM polarized incident light. The insets are schematic description for polarization: (a) 2D pattern and (b) 3D pattern.

monochromatic incident photon-to-electron conversion (IPCE) has been investigated as shown in Fig. 3(b). It should be noted that J_{sc} values determined by integrating the IPCE data with the AM 1.5G reference spectrum are similar to the ones obtained using J-V measurement with error less than 5%. Therefore, the IPCE results are confirmed to be reliable before measurement. Furthermore, from the IPCE results, we find that there is a clear increment when the 2D and 3D nanopatterned plasmonic back reflector are introduced into the OSCs. Importantly, the IPCE enhancement of OSCs with 3D nanopatterned back reflector is superior to that of the 2D nanograting back reflector, which is consistent with the absorption result from Fig. 3(a). Consequently, the observed absorption enhancement via plasmonic nanostructures, particularly the 3D nanograting, contributes significantly to the enhancements of J_{sc}, IPCE, and PCE along with the improved electrical properties of increased interfacial area.

Furthermore, we find that 3D grating device has a polarization-insensitive response, which is another advantage of 3D nanopatterned back reflector apart from its more efficient PCE enhancement compared to the 2D nanograting back reflector (see Fig. 5). Optical reflection measurements are performed at 15° incidence for two different polarizations, electrical field perpendicular (TM) and parallel (TE) to the pattern direction (y-axis, see the insets in Fig. 5). Fig. 5(a) shows the measured reflection ratio (reflection of TE polarized light/reflection of TM polarized light) of 2D and 3D nanopatterned devices excited for TE and TM polarization, respectively. There is a strong peak around 700 nm (red line in Fig. 5(a)), which is attributed to the excited SPR mode induced by the 2D metallic back grating excited by TM polarized light (Fig. 4(a)) and not by TE polarized light (Fig. 4(b)). Under TE polarization, where the E-field is parallel to the grating direction (y-axis), the grating arrays behave as ineffective plasmon media, so the extinction is not as strong as for the case of TM polarization. Thus, the response of 2D device is very sensitive to the incident polarization. In contrast, after introducing the 3D nanopatterned back reflector with x- and y-axis symmetry and similar periodicity to 2D grating, the extinction spectra do not depend on the incident polarization which is also confirmed by near field profiles as shown in Figs. 4(e) and 4(f). As a result, incident light with E-field parallel to x-axis or y-axis will both excite SPR modes, and the reflection ratio of 3D grating case are almost equals 1 in the whole considered wavelength range as shown by blue line in Fig. 5(a), respectively. Similar trends can also be observed in the IPCE ratio (IPCE of TM polarized light/IPCE of TE polarized light) as shown in Fig. 5(b). Consequently, these results (reflection ratio and IPCE ratio) clearly indicate that the 3D patterned devices not only achieve a more efficient PCE but also possess a polarization-independent response, which will significantly improve its performance and greatly extend its use in photovoltaic applications.

In conclusion, a larger light-trapping effect and thus a more efficient PCE enhancement by 24.6% has been realized by adopting a 3D plasmonic nanopatterned back reflector in OSCs (only 17.5% PCE enhancement for 2D patterned device). The efficient enhancement can be attributed to SPR mode induced by the 3D plasmonic reflector and increased interfacial area. Moreover, compared with the 2D grating design, the 3D patterned design shows a polarization-independent response due to the symmetric arrangement of 3D array geometry. The results contribute to the geometrical design of nanostructured back reflector for higher-efficiency and polarization-insensitive plasmonic OSCs.

This work was supported by University Grant Council of the University of Hong Kong (Grant No. 201111159062), GRF grants (Nos. HKU712010E and HKU711612E), and RGC-NSFC grant (No. N_HKU709/12) from the Research Grants Council of Hong Kong Special Administrative Region, China.

[1]M. Kauranen and A. V. Zayats, Nat. Photonics **6**(11), 737–748 (2012).
[2]G. Li, R. Zhu, and Y. Yang, Nat. Photonics **6**(3), 153–161 (2012).
[3]A. P. Kulkarni, K. M. Noone, K. Munechika, S. R. Guyer, and D. S. Ginger, Nano Lett. **10**(4), 1501–1505 (2010).
[4]X. H. Li, W. C. H. Choy, L. J. Huo, F. X. Xie, W. E. I. Sha, B. F. Ding, X. Guo, Y. F. Li, J. H. Hou, J. B. You, and Y. Yang, Adv. Mater. **24**(22), 3046–3052 (2012).
[5]X. Li, W. C. H. Choy, H. Lu, W. E. I. Sha, and A. H. P. Ho, "Efficiency Enhancement of Organic Solar Cells by Using Shape-Dependent Broadband Plasmonic Absorption in Metallic Nanoparticles," Adv. Funct. Mater. (published online).
[6]D. Madzharov, R. Dewan, and D. Knipp, Opt. Express **19**(6), A95–A107 (2011).
[7]K. S. Nalwa, J. M. Park, K. M. Ho, and S. Chaudhary, Adv. Mater. **23**(1), 112–116 (2011).
[8]D. H. Wang, J. Seifter, J. H. Park, D. G. Choi, and A. J. Heeger, Adv. Energy Mater. **2**(11), 1319–1322 (2012).
[9]W. L. Bai, Q. Q. Gan, G. F. Song, L. H. Chen, Z. Kafafi, and F. Bartoli, Opt. Express **18**(23), A620–A630 (2010).
[10]E. Lee and C. Kim, Opt. Express **20**(19), A740–A753 (2012).
[11]A. Naqavi, K. Soderstrom, F. J. Haug, V. Paeder, T. Scharf, H. P. Herzig, and C. Ballif, Opt. Express **19**(1), 128–140 (2011).
[12]B. Niesen, B. P. Rand, P. Van Dorpe, D. Cheyns, L. Tong, A. Dmitriev, and P. Heremans, Adv. Energy Mater. **3**(2), 145–150 (2013).
[13]X. H. Li, W. E. I. Sha, W. C. H. Choy, D. D. S. Fung, and F. X. Xie, J. Phys. Chem. C **116**(12), 7200–7206 (2012).

Downloaded 17 Apr 2013 to 147.8.236.116. This article is copyrighted as indicated in the abstract. Reuse of AIP content is subject to the terms at: http://apl.aip.org/about/rights_and_permissions

[14]J. You, X. Li, F.-x. Xie, W. E. I. Sha, J. H. W. Kwong, G. Li, W. C. H. Choy, and Y. Yang, Adv. Energy Mater. **2**(10), 1203–1207 (2012).
[15]H. A. Atwater and A. Polman, Nat. Mater. **9**(3), 205–213 (2010).
[16]T. Sondergaard, S. M. Novikov, T. Holmgaard, R. L. Eriksen, J. Beermann, Z. H. Han, K. Pedersen, and S. I. Bozhevolnyi, Nat. Commun. **3**, 969 (2012).
[17]L. Muller-Meskamp, Y. H. Kim, T. Roch, S. Hofmann, R. Scholz, S. Eckardt, K. Leo, and A. F. Lasagni, Adv. Mater. **24**(7), 906–910 (2012).
[18]A. Baba, N. Aoki, K. Shinbo, K. Kato, and F. Kaneko, ACS Appl. Mater. Interfaces **3**(6), 2080–2084 (2011).
[19]X. Y. Duan, S. Q. Chen, H. F. Yang, H. Cheng, J. J. Li, W. W. Liu, C. Z. Gu, and J. G. Tian, Appl. Phys. Lett. **101**(14), 143105 (2012).
[20]L. Li, Y. Yang, and C. H. Liang, J. Appl. Phys. **110**(6), 063702 (2011).
[21]W. E. I. Sha, W. C. H. Choy, and W. C. Chew, Opt. Lett. **36**(4), 478–480 (2011).
[22]H. X. Xu, G. M. Wang, M. Q. Qi, J. G. Liang, J. Q. Gong, and Z. M. Xu, Phys. Rev. B **86**(20), 205104 (2012).
[23]Y. Liu, R. Dhakal, V. Dalal, and J. Kim, Appl. Phys. Lett. **101**(23), 233904 (2012).
[24]C. M. Hsu, C. Battaglia, C. Pahud, Z. C. Ruan, F. J. Haug, S. H. Fan, C. Ballif, and Y. Cui, Adv. Energy Mater. **2**(6), 628–633 (2012).

Downloaded 17 Apr 2013 to 147.8.236.116. This article is copyrighted as indicated in the abstract. Reuse of AIP content is subject to the terms at: http://apl.aip.org/about/rights_and_permissions